Thirty Years of Atmospheric Extinction from Telescopes of the North Atlantic Canary Archipelago

BENJAMIN A. LAKEN

Department of Geosciences, University of Oslo, Oslo, Norway

HANNU PARVIAINEN

Department of Physics, Oxford University, Oxford, England

ALEJANDRO GARCÍA-GIL

Agencia Estatal de Meteorología, Izaña Atmospheric Research Center, Santa Cruz de Tenerife, and Instituto de Astrofísica de Canarias, San Cristóbal de La Laguna, Tenerife, Spain

CASIANA MUÑOZ-TUÑÓN, ANTONIA M. VARELA, SERGIO FERNANDEZ-ACOSTA, AND PERE PALLÉ

Instituto de Astrofísica de Canarias, and Department of Astrophysics, Universidad de La Laguna, San Cristóbal de La Laguna, Tenerife, Spain

(Manuscript received 31 July 2014, in final form 23 April 2015)

ABSTRACT

This study examines 30 years of atmospheric extinction, τ, obtained from both stellar and solar telescope measurements, at ~2.4 km MSL, from the North Atlantic Canary Archipelago—an island chain located at approximately 28°N, around 100 km from the west coast of Africa. Data from three AERONET monitors, located at varying heights on one of the main islands, were also used, although these are only available over a shorter (<10 yr) period. The Canary Archipelago is regularly affected by dust intrusions into the local atmosphere as they intersect one of the primary export pathways of mineral dust from the Sahara. The τ of "baseline" and "dust influenced" conditions were statistically distinguished by fitting normal-gamma mixture distributions to the observations using Markov chain Monte Carlo methods, and then the seasonal and long-term characteristics of these data were examined. The telescope data show that baseline conditions are usually stable at $\tau < 0.1$ (except during periods influenced by volcanic aerosols) and indicate the existence of a low-amplitude ($\tau = 0.01$) seasonal variation. During dust-influenced conditions, τ regularly reaches values of a factor of 2–6 times higher than normal. The majority of dust intrusions take place during the months of July and August, when they may occur 44 ± 15% of the time, predominantly at high altitudes (with ~94.3 ± 1.6% of intrusions occurring ≥ 2.4 km), whereas during the months of November–May, dust intrusions occur far less frequently (~19 ± 7%) and are more common at lower altitudes—with intrusions at <2.4 km comprising ~ 79.5 ± 3.2% of all outbreaks. Year-to-year variations in the frequency of dust-influenced conditions (of ~9%) were found but no long-term trend over the observed 30-yr period.

1. Introduction

Telescopes have made routine astronomical observations at sites across the world for decades. These instruments are usually located in areas of the highest quality with regard to low levels of light and air pollution, and a high frequency of clear-sky days. The Canary Archipelago, located approximately 100 km west of the North African coast, is home to two such observatories, both managed by the Instituto de Astrofísica de Canarias (Spain): Observatorio del Teide, located on the island of Tenerife (28.3°N, 16.50°W; 2.4 km MSL); and Observatorio del Roque de los Muchachos, located on the island of La Palma (28.46°N, 17.53°W; 2.4 km MSL).

Denotes Open Access content.

Corresponding author address: Benjamin A. Laken, Department of Geosciences, University of Oslo, P.O. Box 1022, Blindern, 0315 Oslo, Norway.
E-mail: blaken@geo.uio.no

DOI: 10.1175/JCLI-D-14-00600.1

Numerous parameters can be calculated from telescope data, such as atmospheric extinction (τ)—the magnitude (logarithmic brightness) in a specified wavelength band, attenuated along a given path per unit of air mass. For the astrophysics community, these data are primarily used to correct for the effects of the local atmosphere on astrophysical observations and are usually thought of as uninteresting in themselves. Because of the long operation of telescope instruments, large volumes of atmospheric data of potentially invaluable utility to the atmospheric science community have been accumulated. In particular, because of the proximity of the archipelago to the western Sahara and the frequent impact of dust-laden winds, τ measured from the Canary Archipelago is useful for studying mineral dust aerosols—the impacts of which are readily apparent in records derived from telescope data (e.g., Guerrero et al. 1998; Jiménez et al. 1998; Varela et al. 2004; García-Gil et al. 2010). Such records may assist in improving our understanding of the processes and impacts related to Saharan mineral dust on the earth's climate system. Such improvements are needed as currently even basic aspects of the emission and transport of dust are not reproduced by state-of-the-art global climate models (Evan et al. 2014).

This current work builds upon the approach of Laken et al. (2014), who used data of nightly averaged measurements of τ from one telescope located on the island of La Palma to examine the frequency of mineral dust outbreaks in the local atmosphere. We have improved upon these results by utilizing multiple telescopes, with simultaneous measurement techniques, recorded over all times of day (solar observations during daytime and stellar observations at nighttime). In this work, we construct a homogeneous record of τ over the 1985–2013 period and describe the behavior of these data over seasonal and annual time scales. We also compared these data to (shorter) records obtained from three Aerosol Robotic Network (AERONET) sites located on the island of Tenerife.

2. Sources of data

a. Carlsberg Meridian Telescope

We have utilized nightly values of τ, derived from the Carlsberg Meridian Telescope (CMT) of the Observatorio del Roque de los Muchachos, similar to earlier studies (e.g., Guerrero et al. 1998; Jiménez et al. 1998; Varela et al. 2004; García-Gil et al. 2010; Laken et al. 2014). These data (available from http://www.ast.cam.ac.uk/~dwe/SRF/camc_extinction.html) are calculated from routine observations of stars over the course of a night.

Two different methods of measurement were used to make the observations at different time periods: the first method calculated a single nightly average of τ from ~56 photometric standard stars per night as they crossed the north–south meridian, with a nightly standard deviation of ±38 stars. These data were recorded from 13 May 1984 until 28 May 1998, in the 551-nm Johnson visual (V)-band at zenith, using a scanning slit micrometer (SSM).

The later, more sophisticated measurement method, used from 26 March 1999 onward, employed a charge-coupled device (CCD) instrument, operating at 625 nm in the Sloan Digital Sky Survey r' band; this instrument took numerous images over the course of a night, each with around 30–40 photometric standard stars within the field of view. Unlike the earlier measurements, extinction is calculated for each good (photometric) frame of data. Specifically, photometric data are the measurements that have a constant low degree of scattering (<0.15 magnitude) over the course of the night's observation, and also a low degree of scattering (<0.06 magnitude) between the photometric standard stars in each frame of recorded data. We note that these data may be made under partially cloudy conditions if sufficient (>9) photometric standard stars are still observable. Further information regarding these measurement techniques can be found in King (1985).

b. Mark-1 instrument

The Mark-1 instrument (a resonant scattering solar spectrophotometer) was designed to measure the radial velocity of the sun (Brookes et al. 1978). It uses monochromatic measurements of the intensity of sunlight at the blue and red wings of the neutral potassium (K I) line at 769.9 nm; further details can be found in Pallé et al. (1986) and Cortés and Pallé (2014) (data are available from http://www.spaceinn.eu/data-access/mark-i-data-archive/). Intensity is calculated via two distinct methods—using transmitted and scattered light; a value of τ may be derived from these data in the manner outlined below, which we illustrate with examples from 21 June 2001 (a boreal solstice date).

1) During clear-sky daylight hours, intensity values of the sun (magnitude m) are recorded from both transmitted and scattered light. The average (μ) and standard deviation (σ) intensity values over 40-s time windows are recorded, along with the time of the observation and positional information of the sun (i.e., declination and ascension).
2) Based on the coordinates of the observatory, the time of observation, and the positional information of the sun, the amount of atmosphere that the

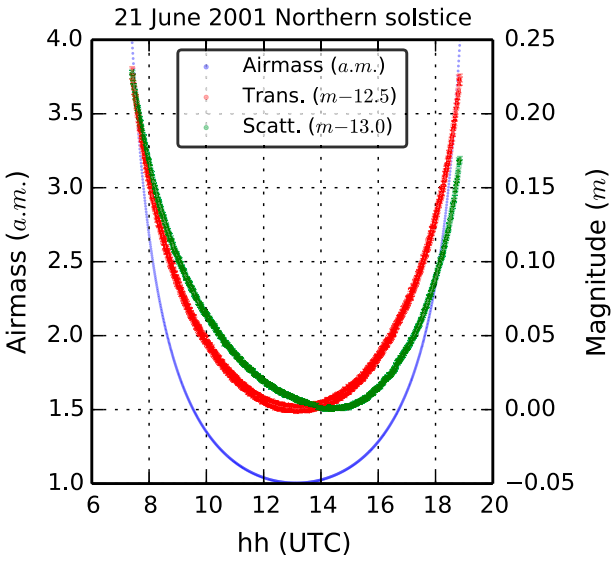

FIG. 1. An example of the 40-s mean (μ) photometric intensity (m) from transmitted and scattered light collected by the Mark-1 instrument, for the observations of 21 Jun 2001. The intensity values (axis on right-hand side) have been normalized to zero. The range surrounding the 40-s μ values indicates the measured $\pm 1\sigma$. The air am is also calculated (blue points); its axis is on the left-hand side.

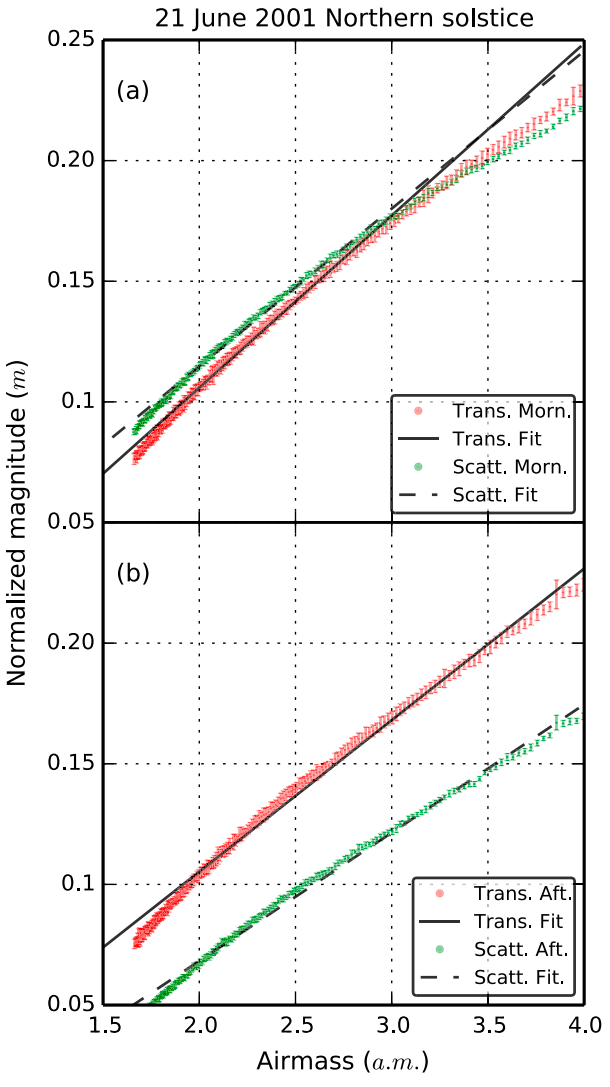

FIG. 2. The normalized magnitude (m) and $\pm 1\sigma$ errors from transmitted and scattered light have been divided into (a) premeridian (morning) and (b) postmeridian (afternoon) periods, and plotted against am for the observations of 21 Jun 2001. Linear regressions weighted by the σ uncertainty are displayed. The slope of the regressions ($m \times \text{am}^{-1}$) are a measure of τ.

sunlight traveled through to reach the telescope is calculated [air mass (am)] from the formula of Hardie (1962)—the lowest airmass values are when the sun is at zenith. We have plotted the air mass along with the normalized magnitude of transmitted and scattered light for 21 June 2001 in Fig. 1.

3) Data are categorized into premeridian and postmeridian times: that is, the time during which the sun is rising, and the light passing through the atmosphere to the east of the Canary Islands (i.e., over the western Sahara) is separated from the time the sun is setting and passing through atmosphere to the west of the islands (i.e., over the North Atlantic Ocean).
4) A linear regression is calculated from the am vs. μ intensity, weighted by the σ of the intensity values, for the premeridian and postmeridian data (Fig. 2).
5) The slope term of each linear regression ($m \times \text{am}^{-1}$) is equivalent to τ. We note that these units may be converted to optical depth using a factor of $2.5 \times \log_{10} e = 1.086$ (e.g., as in Finkbeiner 2003; Krügel 2009). We also calculate the standard error of the mean (SEM), $\sigma\sqrt{(N-1)}$, where N is the sample size of each premeridian and postmeridian group of intensity values. The SEM is used as a measure of the uncertainty for each τ value throughout this work.

There are several particulars of the data reduction that require further elaboration. The relationship between time and intensity is logarithmic, whereas the relationship between air mass and intensity is linear. Consequently, the majority of observations are made at low-airmass values (e.g., as seen for our examples of 21 June 2001, shown in Fig. 3). However, there are some points to consider regarding the processing of low-airmass data for our purposes (i.e., the creation of a consistent time series of τ). For measurements in scattered light, a bias exists in the data points at airmass values, am < 1.25. This is visible in Fig. 1 as a deviation in the behavior of the scattered data from the transmitted values at low am values; the reason for this is

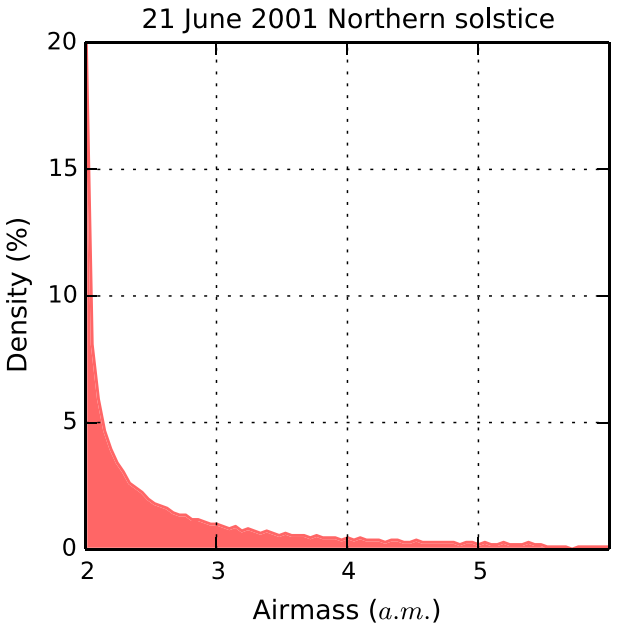

FIG. 3. Density of the population of data points at a given am value for the example of the observations of 21 Jun 2001.

explained in Cortés and Pallé (2014). However, for our purposes, low-airmass values are relatively unimportant as it is light that has traveled along longer paths and that has had greater opportunity to encounter absorbing and scattering aerosols that can give us the most information about the earth's atmosphere. Ironically, this is the opposite of the requirements of astrophysicists, who would seek to discard data at high-airmass values for the very reason of atmospheric interference. In addition to the bias at low am values in scattered light, there is further consideration: the lowest am values change seasonally (Fig. 4)—this seasonality results from the change in the sun's zenith angle—which could produce an artificial seasonality in the τ values. Consequently, the lowest am values we use to calculate daily τ values are above the seasonal variation, am >1.62 (this is the reason for the removal of lower am values, apparent in Fig. 2).

c. AERONET

The aerosol optical depth (τ_a), the degree to which aerosols prevent the transmission of light, of a specified wavelength, along a given path by the absorption and scattering, is a quantity calculated from the sun photometer data of AERONET. They measure a range of wavelengths that have been shown to be sensitive to mineral dust intrusions (e.g., Müller et al. 2003). Although consistent AERONET data are only available for the Canary Islands since 2004 (specifically the island of Tenerife), the short records they provide are useful as an independent verification to the telescope measurements. Additionally, because of the different altitudes of the AERONET stations, these data may also provide some indications regarding the characteristics of the altitude of mineral dust events—a factor known to be important in controlling the vertical heating of the local atmosphere (Westphal et al. 1987).

There are three AERONET instruments on the island of Tenerife, closely located horizontally, but with large differences in altitude. Specifically, the three sites are at Santa Cruz (28.473°N, −16.247°E; 52 m MSL; available since 18 July 2005), La Laguna (28.482°N, −16.321°E; 568 m MSL; available since 16 July 2006), and Mt. Teide (28.309°N, −16.499°E; 2391 m MSL; available since 26 June 2004). For this work we have used the level 2.0, daily summary, quality-assured data, at the 675-nm wavelength.

These stations require clear-sky conditions to operate. Because of the influences of topography and prevailing winds, there are strong microclimates over the island of Tenerife; consequently, there are large variations in the average number of observed (clear sky) days at each of the three AERONET sites as follows: Santa Cruz, 21.6 ± 0.8 days month^{-1}; La Laguna, 18.9 ± 0.8 days month^{-1}; and Mt. Teide, 24.1 ± 0.6 days month^{-1}.

THE RELEVANCE OF SATELLITE DATA

Satellite data are highly useful in characterizing atmospheric mineral dust aerosols, particularly for the identification of key locations of mineral dust entrainment and large-scale dynamics (e.g., Moulin et al. 1998; Evan and Mukhopadhyay 2010). These data are invaluable as regions of key importance to mineral dust tend to be areas with limited surface-based measurements (Knippertz and Todd 2012). For many locations across the globe, such as deserts and ocean regions, satellites are the only reliable source of long-term (~30 yr) data. However, these data have significant limitations, particularly with respect to their long-term homogeneity. There are also significant limitations to the temporal and spatial sampling available, whereby the high-spatial resolution of polar-orbiting satellites is accompanied by a poor-temporal resolution (and vice versa for geostationary satellite instruments). As a result of these and additional issues—such as distinct view angles from ground-based instruments—a direct comparison between satellite measurements and the ground-based telescope data presented in this work is problematic.

Indeed, poor agreement between in situ optical depth observations and satellite data have been reported in comparisons of atmospheric extinction from telescopes of the Canary Islands to corresponding satellite data from both the Total Ozone Mapping Spectrometer (TOMS) Ozone Monitoring Instrument (OMI), and the *Terra*/*Aqua* Moderate Resolution Imaging Spectroradiometer (MODIS) (Varela et al. 2008).

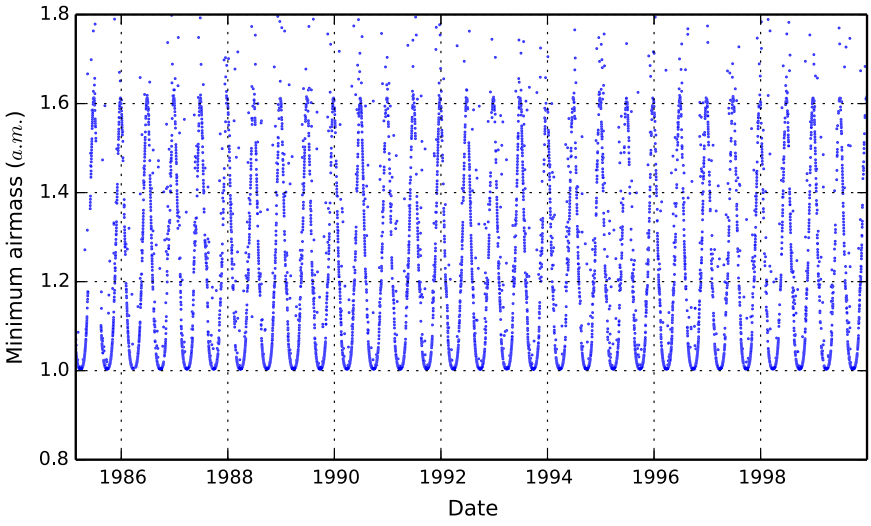

FIG. 4. The minimum am value of each observed calendar day of the Mark-1 instrument. The strong seasonality is due to the relative change in the position of the sun at zenith.

The study found that the satellite data showed no linear agreement between the telescope and satellite data, but weak correlations were found during summertime measurements. Varela et al. (2008) concluded that this disagreement was largely due to the different viewing perspectives of the instruments. The authors also noted that local-scale climate factors played an important role in producing conditions at the observation site that were distinct from those of the wider area (estimated by the satellite instrument). Consequently, while satellite-based analysis of mineral dust aerosols is a critical avenue for advancement in our understanding of aerosols, these data are significantly distinct from the in situ observations presented in this work; hence, we have not utilized satellite data in this study.

3. Methods

a. Individual datasets from telescope sources

We have six distinct time series of τ from the telescope data: two from stellar observations of the CMT covering different time periods (with much reduced error in the later measurements) and two (simultaneous) series—in transmission and scattering—during morning and afternoon, from the Mark-1 instrument. Unfortunately, the transmission data end in late 2005 due to instrumental failure. All of these individual time series are plotted together in Figs. 5a–c. Prior to their use, the CMT data were corrected to the equivalent wavelength of the Mark-1 instrument (769.9 nm) using the correction values of King (1985). From initial examination, these data show good agreement, indicating that conditions are usually stable at $\tau < 0.1$ all year at the height of the observatories, with the exception of sporadic high-magnitude variations clustered around summer months, during which time τ regularly reaches values that are a factor of 2–6 times higher than normal.

These data are also displayed as density plots (Figs. 6a–c), which indicate the proportion of the values (%) that fall within a given range of τ values. There are several features that should be noted in the density plots: First, these data are made up of a normally distributed component centered around low ($\tau < 0.1$) values and a long positive tail (gamma distribution). The normally distributed component (which we shall also refer to in this work as "baseline conditions") results from the regular state of the local atmosphere around the Canary Islands (i.e., conditions in the absence of a mineral-dust-loaded atmosphere), whereas the long positive tail results from the influence of mineral dust suspended in the local atmosphere. The idea that baseline and dust-influenced τ values may be statistically separated has been explored by several authors (e.g., Guerrero et al. 1998; Jiménez et al. 1998; Siher et al. 2004; García-Gil et al. 2010); although, these studies were limited as they did not consider long-term changes in baseline τ conditions (Laken et al. 2014).

The second feature of interest in the density plots is a comparison of the changing distribution identified at different times of day and with different measurement methods (Fig. 6). We find that the broadest distribution is that of the early CMT measurements, which used a silicone strip detector (SSD)-based instrument. We also note that these measurements have low sensitivity, leading to the coarse categorization of τ values, whereas the later, more sophisticated, CMT CCD measurements are in better agreement with the Mark-1 data. The

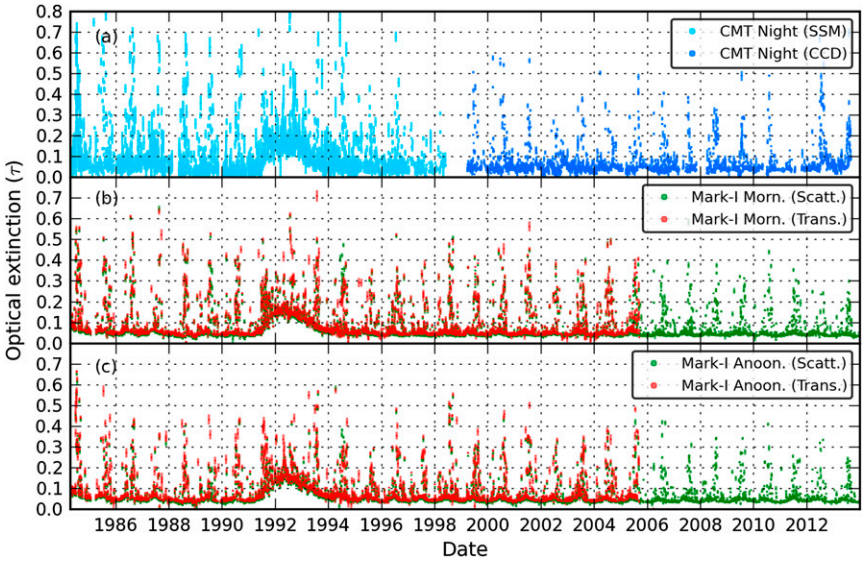

FIG. 5. The time series of τ calculated from individual telescope datasets are presented, distinguished by telescope, times, and method. (top) Nightly averaged data from the CMT recorded using an SSM (light blue) and then the CCD (dark blue) method. The CMT data intensity values have been adjusted to 769.9-nm equivalents. (middle) Mark-1 morning and (bottom) afternoon data from both scattering (green) and transmission (red). All data points are $m \times \text{am}^{-1}$ with the error bars showing the RMSE (m).

median values of the distributions are 0.047 ± 0.005 τ. Interestingly, the Mark-1 afternoon distributions show slightly lower (and less peaked) modal values than their morning counterparts, with afternoon values being 0.052 and 0.044 τ versus 0.053 and 0.046 τ in the morning (for transmission and scattering, respectively); the nightly extinction values from the CMT lie between these values. This result is likely due to a physical difference in the baseline aerosol conditions of local atmosphere, as the light of the morning extinction data travels over the atmosphere overlying North Africa, whereas afternoon light travels through atmosphere overlying the North Atlantic. Consequently, the mornings have a higher and more consistent dust loading than the afternoons (and thus both a higher and more peaked modal value).

b. *Population fitting method*

A normal-gamma mixture distribution is used to model the population of the extinction values. We fit the theoretical distribution to the observed atmospheric extinction values over a specified interval (e.g., the whole population, or a 100-day moving window) by using a Bayesian approach, computing the posterior probability distributions for the mixture distribution parameters using a Markov chain Monte Carlo (MCMC) procedure.

The distribution is a linear combination of a normal distribution (modeling the extinction variability of regular atmospheric conditions), combined with a gamma distribution (to model the long positive tail caused by the mineral dust conditions). Namely, the mixture distribution for τ is $P(\tau; \mu, \sigma, o_g, a_g, b_g, c)$, where μ and σ are the mean and standard deviation of the normal distribution, respectively; o_g, a_g, and b_g are the origin, shape, and width of the gamma distribution, respectively; and c is the mixing factor. An example of this fitting procedure is given in Fig. 7 for the CMT CCD data, with the 50th and 99.9th percentile values of the normal distribution highlighted.

Uninformative constant priors are used on all the distribution parameters, and the likelihood is expressed directly as the product of the probabilities for obtaining each τ value from the composite distribution. Based on the μ and σ posteriors of the normal component of the composite distribution, we may identify key features of the populations. For example, in Fig. 8 we have used this method to plot the 50th percentile probability (i.e., modal) values of the normal component of the distribution. In a following section, we will use the distributions to construct a high-pass filter (HPF) to identify the 99.9th percentile probability value of the normal distribution as the point at which we consider all higher values to be outside the range of baseline variability, and thus indicate a day where mineral dust was present in the local atmosphere. Using the MCMC fitting technique, we find that the 99.9th percentile values of the normally distributed components within the six density plots of Fig. 6 are 0.083 ± 0.013 τ (we note these data cover the entire available observation period excluding volcanic years and

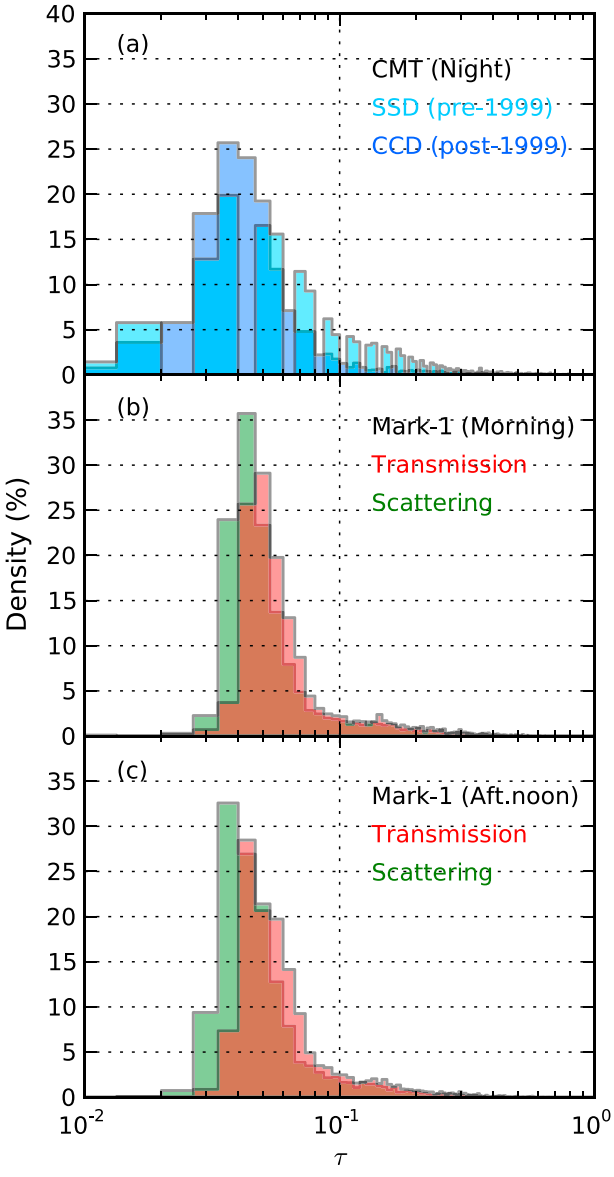

FIG. 6. Filled histograms showing the density (%) of the data points over a given value of τ for the identical data in Fig. 5.

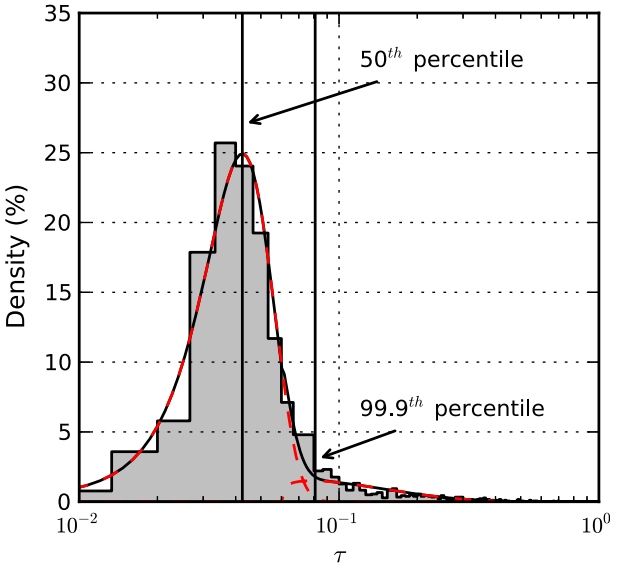

FIG. 7. Example of the MCMC fitting process to the τ populations (for the case of CMT CCD data). Gray-filled histogram shows the density of data points at given τ values, red dashed lines show MCMC fits to the normal and gamma components of the populations, and the black smoothed line shows the combined model fit. Vertical black lines show the 50th and 99.9th percentile values from the fit to the normally distributed component of the population.

are calculated from intensity at 769.9 nm). Generally, values beyond this threshold can be considered to be influenced by the suspended mineral dust; however, we note that this threshold is sensitive to change over time with baseline τ conditions (particularly as a result of the influence of volcanic stratospheric aerosol influence).

4. Analysis

a. *Accumulated time series*

Each of the six time series of Fig. 5 has benefits and limitations. In addition to the differing performance of both the measurement methods of the CMT and Mark-1, extinctions calculated from different positions, observing different directions of the sky, and at different times of the day may result in a range of distinct biases (as noted in section 3). Additionally, artificial biases related to errors in the fitting of air mass to the apparent brightness of an object may also be a factor influencing τ calculated at distinct periods of the day (e.g., Cachorro et al. 2004, 2008). Consequently, we have combined the individual time series together to create a more robust dataset, shown in Fig. 8, that represents the τ and error over the region of the Canary Islands during a period of approximately 24 h. This was accomplished by averaging the available τ values over a calendar day and accumulating the RMSE. To these data, we have used the MCMC fitting procedure previously described to fit the 50th and 99.9th percentile values of the normally distributed data component, over a 100-day moving window (as explained in section 3). We consider any value that exceeds the 99.9th percentile value across the accumulated data to indicate dust-influenced conditions.

A clear benefit of accumulating the data is also the data coverage achieved. Individually, the telescope observations are restricted to certain times of day and have varying coverage over the observation period; accumulating the data achieves a nearly full coverage over the 1984–2014 period (with a monthly average of

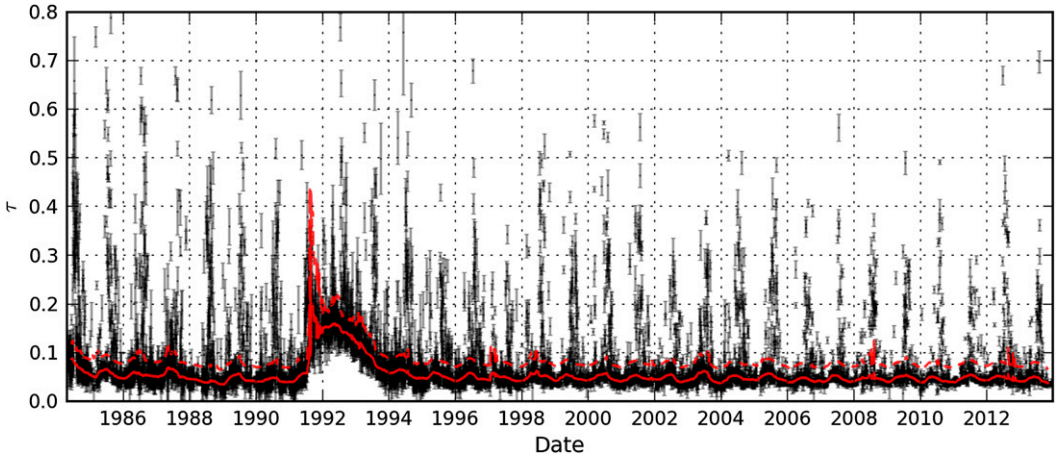

FIG. 8. Accumulated τ values and SEM uncertainties from the six time series presented in Fig. 5. The solid and dashed red lines show a running 100-day (box car) MCMC-calculated fit to the 50th and 99.9th percentile values, respectively, of the normally distributed component of the data.

30.04 ± 0.18 days month^{-1}). An initial analysis of the accumulated τ data shows a number of prominent features:

1) The most common extinction values are low ($\tau < 0.1$) and demonstrate possible seasonal variability, yet are stable over long (>1 yr) time scales. The data points are readily distinguishable from the considerably higher τ values associated with mineral dust events centered around summer months.
2) The impact of stratospheric aerosols from the Mt. Pinatubo volcanic eruption in 1991 is evident as a strong increase in the normally distributed (nondust related) τ component, over a period of roughly 3 yr, increasing extinction by $\sim 0.01\tau$—approximately doubling baseline values. It is also probable that the eruption of El Chichón in 1982 also influenced the start of the records as τ values were initially anomalously high (both features have been previously noted from telescope data of La Palma; e.g., Guerrero et al. 1998; García-Gil et al. 2010).

To explore the seasonal behavior of the accumulated data, we have plotted the daily τ values of the 1984–2014 period by their day-of-year (DOY) occurrence (Fig. 9a)—the years associated with the El Chichón and Mt. Pinatubo eruptions were excluded. These data show that the influence of mineral dust outbreaks on the local atmosphere of the Canary Islands is largely confined to the June–October period, during which time τ values from ~0.1–0.7 may occur. Prior to this, a less-frequent and less-intense period of outbreaks also occurs during the months of February–April.

Strong seasonal variations in the latitudinal export of mineral dust from the Sahara are well known (e.g., Janowiak 1988; Swap et al. 1996; Moulin et al. 1997; Goudie and Middleton 2001). However, regarding the seasonality of the dust outbreaks, there is an important point to consider: qualitative observations and local experience suggest that dust outbreaks occur below the height of the telescopes, and consequently are not observed (Varela et al. 2008). If the height of the dust outbreaks varies with a seasonal component, then this would introduce a bias in the data. This is likely as during summer dust outbreaks tend to occur in the free troposphere (Cuesta et al. 2009), whereas in winter outbreaks more frequently occur in the marine boundary layer (MBL) as a result of anticyclonic activity (Viana et al. 2002; Alonso-Pérez et al. 2011). Consequently, it is likely that at least some of the seasonality observed in the dust outbreaks from telescopes is due to measurement bias (we will consider this further shortly).

Two further limitations to both the telescope and AERONET measurements with regard to identifying dust outbreaks should also be mentioned. First, even if the dust outbreaks are of a sufficiently high altitude to be observed by the telescopes, they can also be of a highly localized nature, having a clearly defined boundary (e.g., Cana 2002). Consequently, telescopes may miss dust outbreaks if they fail to intersect the path of light that the telescopes are observing (e.g., Varela et al. 2008). Second, dust outbreaks in the marine boundary layer have also been noted in association with anticyclonic conditions (e.g., Varela et al. 2008; Alonso-Pérez et al. 2011): in cases where the mineral dust aerosols are underlying (or mixed with) cloud cover above the height of the instruments, no observations are made.

Although the properties of the dust outbreaks are readily apparent in Fig. 9a, the baseline conditions appear to be homogenous. We have further examined the

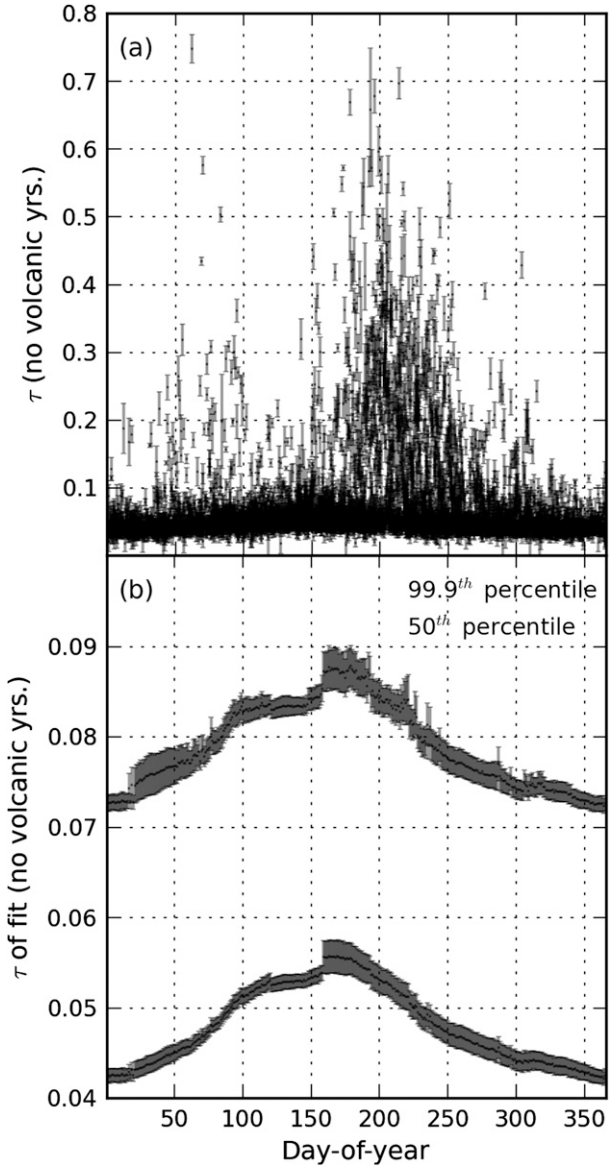

FIG. 9. Plot of the DOY occurrence of (a) the accumulated τ and (b) the mean (and SEM range) of the 50th and 99.9th percentile values of the MCMC-calculated fit to the normally distributed component of the accumulated τ data. Data points during years influenced by El Chichón and Mt. Pinatubo were excluded.

baseline conditions by plotting the DOY $\mu\pm$ 1 SEM τ values of the 50th and 99.9th percentile MCMC fits (i.e., the solid and dashed red lines, respectively, in Fig. 8). These data are presented in Fig. 9b and essentially show the long-term (100-day smoothed) behavior of the baseline conditions from the accumulated data. From these data, we find that a small rise in τ occurs from winter to summer, of 0.042 ± 0.001 to 0.056 ± 0.0018 for the 50th percentile values. It is unlikely that this variation is physical, but instead it is likely to be a residual artifact from low-airmass bias in summer; that is, despite our attempt to homogenize the data, some summertime low-airmass bias likely remains, resulting in elevated τ values (of around 0.01). We also observe the DOY variation is not smooth, particularly for the 99.9th percentile values, with small discontinuities of $\pm 0.005\tau$ frequently occurring. These small differences are caused by instances where the MCMC fitting procedure has slightly overestimated the size of the normal distribution; this overestimation relates to our conservative threshold (the 99.9th percentile) and the consequent amount of overlap between the dust-free, dust-influenced populations. By selecting a conservative threshold, we are biased toward type 1 errors—that is, we more frequently consider a dust-influenced day as a dust-free day than vice versa—as the weakest dust events will be included within the normal distribution (as shown in Fig. 8).

b. *AERONET analysis*

As described in section 2, we use τ_a data from three available AERONET monitors on the island of Tenerife, located closely in horizontal space yet with large differences in vertical position above mean sea level. Time series from the three sites are plotted in Fig. 10, for Mt. Teide, 2391 m, green points (Fig. 10a); La Laguna, 568 m, red points (Fig. 10b); and Santa Cruz, 52 m, blue points (the relationship between the colors used and the specific stations are maintained throughout all subsequent figures; Fig. 10c). We have overplotted the 50th percentile fits (black lines). These data are also presented in Fig. 11, plotted by their DOY occurrence as both the individual τ_a values (Fig. 11a) and the 50th and 99.9th percentile fits (Fig. 11b).

These data show three features of interest. First, a decrease in the baseline values with increasing altitude, from $0.067 \pm 2.3 \times 10^{-4}$ to $0.058 \pm 2.5 \times 10^{-4}$ to $0.017 \pm 6.8 \times 10^{-5}$. This decrease is expected, as the Mt. Teide monitor is situated above the boundary layer, whereas the La Laguna and Santa Cruz sites are within the boundary layer and are also located in urban centers, and thus they should measure significantly higher aerosol concentrations. These differences are most readily apparent in Fig. 11b, with the Mt. Teide DOY 99.9th percentile values appearing below even the 50th percentiles of the La Laguna and Santa Cruz station baseline values for the majority of the year. Second, we find the baseline τ_a conditions of the AERONET sites lack the artificial seasonality identified in the telescope (in Fig. 9b). Third, despite only 6–10 yr of data being available, there is an apparent difference between the seasonal confinement of mineral dust events between the stations: that is, while the Mt. Teide monitor agrees

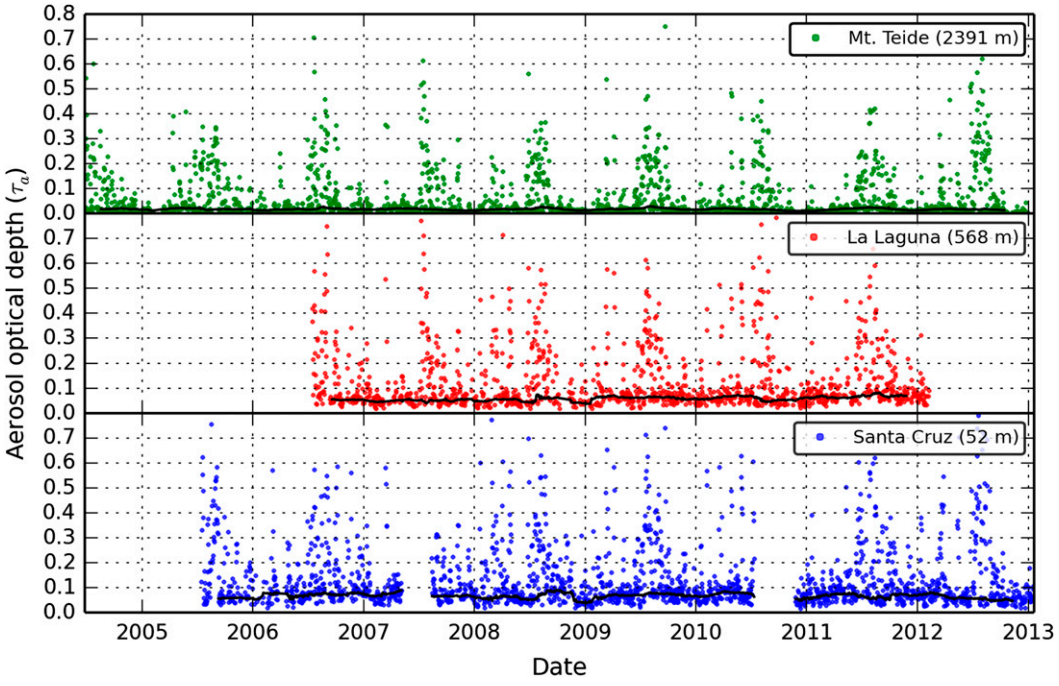

FIG. 10. Level 2.0 quality-assured AERONET daily summary data of a τ_a at 675 nm, from three monitoring sites on the island of Tenerife that are located closely in horizontal space but with large differences in altitudes: (a) Mt. Teide (2391 m), (b) La Laguna (568 m), and (c) Santa Cruz (52 m). Black lines show MCMC-calculated fits to the 50th percentile values, as described in section 3.

with the telescope observations, in that virtually no dust events occur during wintertime, the low-altitude stations (La Laguna and Santa Cruz) show numerous events occurring in wintertime. This supports the hypothesis that part of the seasonality detected in the telescope data is due to a seasonal change in the altitude of mineral dust intrusions, an idea that we will test in the following section.

c. *Dust outbreak height and seasonality*

We wish to consider how the occurrence of dust events changes both seasonally and over long (>1 yr) time scales. To understand this property, we have examined the frequency of dust events per month (a statistic we refer to as f_{dust}). The f_{dust} is calculated from the accumulated data series shown in Fig. 8, by summing the number of days per month where τ exceeded the 99.9th percentile MCMC fit over the time series and then dividing this count by the days per calendar month to create a fraction from 0 to 1; that is, $\tau_{\geq\text{crit}}/N_{\text{mnth}}$, where $\tau_{\geq\text{crit}}$ is the number of days per calendar month, where τ (or τ_a) were found to be above or equal to the MCMC fit to the 99.9th percentile baseline value, and where N_{mnth} is equal to the number of days per calendar month. Consequently, f_{dust} shows the proportion of a given calendar month where dust-influenced conditions are observed.

A seasonal climatology of the f_{dust} statistic is plotted showing data from the accumulated telescopes from 1983 to 2014 (Fig. 12a) and from the accumulated telescope and AERONET where available over their overlapping observation period of 2004–14 (Fig. 12b).

From an examination of the accumulated telescope data over the entire observed period, we observe a strong peak in f_{dust} during the months of July and August of 0.46 ± 0.08 (Fig. 12a). Either side of this peak, the f_{dust} rapidly decreases over a 1–2-month period to ~0.05 ± 0.02. However, examinations of the same data from AERONET show that the period decrease (either side of July and August) is longer, and that the wintertime f_{dust} is higher and more complicated than the telescope data initially reveals (Fig. 12b).

We find that the f_{dust} values of all data points only correspond within a ±1 SEM range during the months of July–September. Although the AERONET observation period is relativity limited, and uncertainty exists in the results from the stations due to differences in the amount of observed days per month, these result suggests that the dust outbreaks frequently occur at high altitudes (approximately >2.4 km) during summer months, although lower-altitude outbreaks also occur (when combined they may occur with a f_{dust} of 0.44 ± 0.15). Furthermore, low-altitude events are persistent throughout the year.

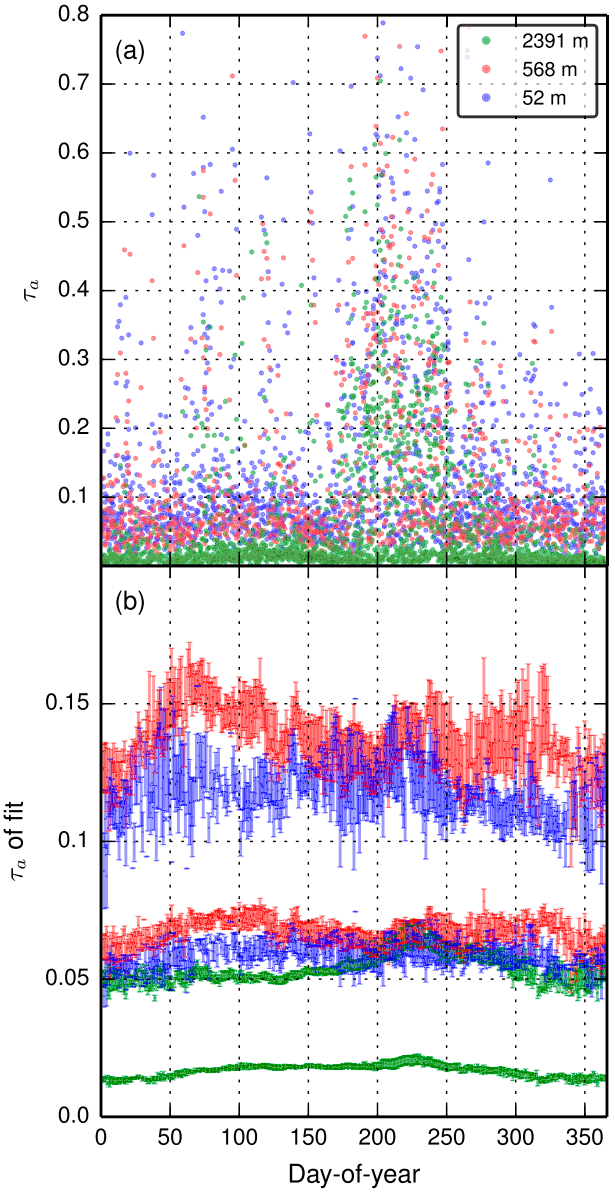

FIG. 11. Plot of the DOY occurrence of (a) the accumulated τ_a and (b) the mean (and SEM range) of the 50th and 99.9th percentile values of the MCMC-calculated fit to the normally distributed component of the accumulated τ_a data.

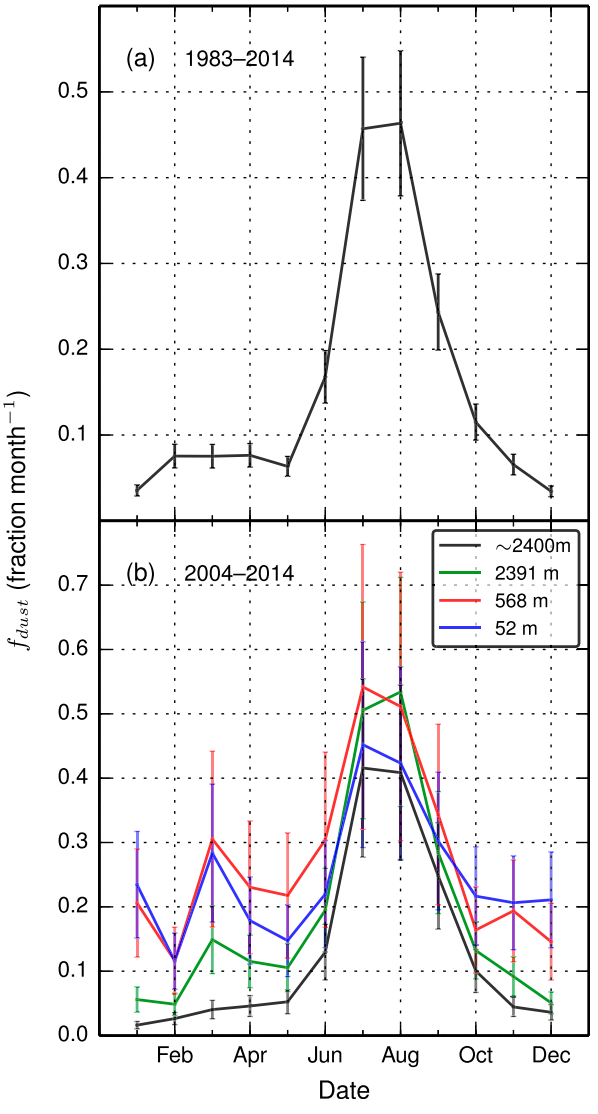

FIG. 12. The f_{dust} (and SEM range) per calendar month (fraction per month) for (a) 1983–2014 accumulated telescope data and (b) accumulated telescope data and AERONET data during ~2004–14. Line colors correspond identically to earlier figures (i.e., black lines are the accumulated telescope data, while colored lines are the AERONET sites of Fig. 10).

We present this result in a slightly different manner in Fig. 13: this figure shows the μ and (and upper limit) f_{dust} both above and below a height of approximately 2.4 km MSL. The figure shows that during the peak summer months (July–August), the vast majority (94.3 ± 1.6%) of outbreaks are at high altitudes (≥2.4 km), whereas during the months of November–May, dust outbreaks occur predominately (79.5 ± 3.1%) at low altitudes (<2.4 km), although with far less frequency than in the summer months ($f_{\text{dust}} \sim 0.19 \pm 0.07$).

d. *Frequency of dust outbreaks versus intensity*

In Fig. 14 we present the relationship between summertime (July–September) dust outbreak frequency (f_{dust}) and the average intensity of the dust-influenced days ($\tau \pm 1$ SEM). We have used a weighted least squares regression to examine the statistical relationships of these data (weighted by the SEM uncertainty of τ). We find that the accumulated telescope data show a weak positive relationship ($r^2 = 0.22$; $y = x \times 1.20 \pm 0.24 + 0.16 \pm 0.06$). This finding is in close agreement with the results obtained from the

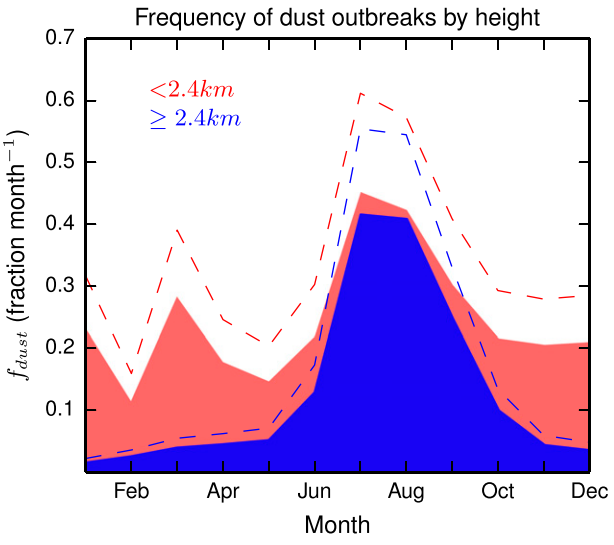

FIG. 13. The f_{dust}, distinguished by the proportion of outbreaks above and below a height of approximately 2.4 km MSL. The <2.4-km data (red shaded region) correspond to data from the Santa Cruz AERONET station, while the ≥2.4-km data (blue shaded region) correspond to the accumulated telescope data. Only data covering the 2004–14 period have been used. The red and blue dashed lines represent the upper (+1) SEM uncertainty range of the data.

AERONET data ($r^2 = 0.29$; $y = x \times 1.05 \pm 0.22 + 0.20 \pm 0.06$).

If we consider that the data points are not independent due to temporal autocorrelation and simultaneous data from each of the AERONET sites, then we may conservatively consider the *df* as the number of years of observations in the data, in which case the r^2 values have two-tailed p values of 0.01 and 0.12, respectively. These results indicate that there is a weak positive relationship between the frequency of summertime dust intrusions and their intensity.

e. *Long-term changes in high-altitude dust outbreak frequency*

As described in section 4, it is only during the months where high-altitude (≥2.4 km) dust outbreaks predominate—the months of July–September—that the telescope data give a reliable estimate of outbreak frequency. Consequently, when performing a long-term analysis of the telescope dataset, we do so only with those months.

In Fig. 15 we show the f_{dust} from 1983 to 2014 during July–September. These data show $\mu = 0.38 \pm 0.07$, $\sigma = 0.09$, and min/max = 0.25/0.58. A linear regression, weighted by the SEM uncertainty, and a 5-yr running mean are overplotted to highlight long-term changes. The 5-yr smoothed values show multiyear variability from around 0.41 to 0.27. Qualitatively, the smoothed values appear to decrease over time. However, despite appearances, the slope is $-1.8 \times 10^{-4} f_{\text{dust}} \text{yr}^{-1}$, resulting in a net linear change over the observation period of only $-5.4 \times 10^{-3} f_{\text{dust}}$, which was not statistically significant.

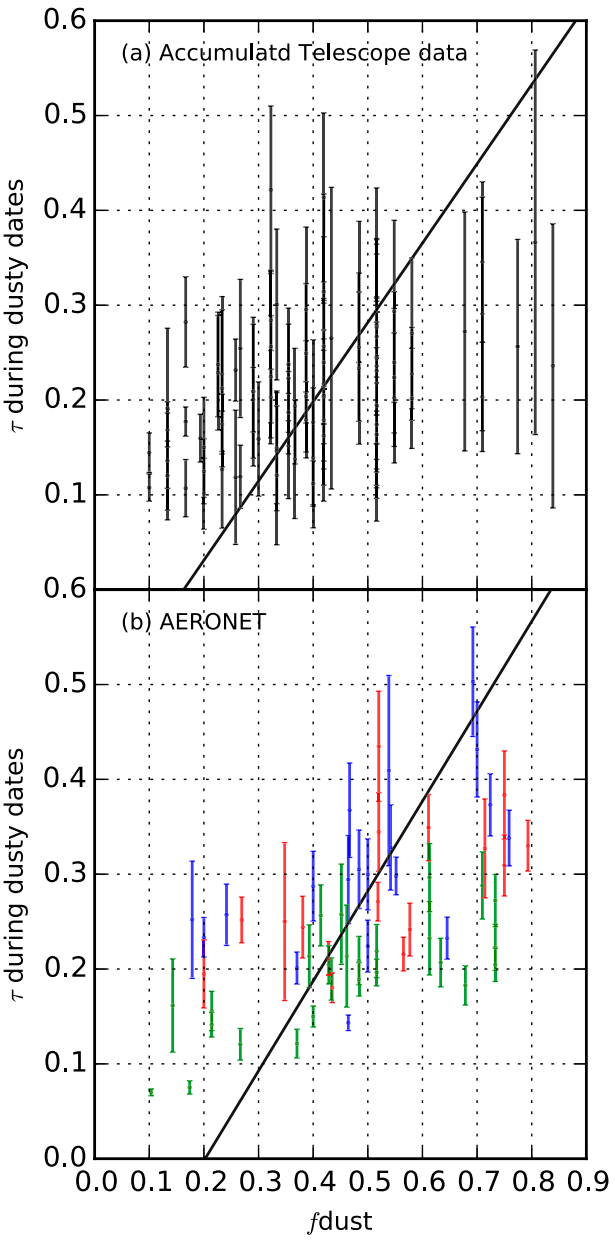

FIG. 14. The f_{dust} from July to September plotted against the intensity (τ) during the dust-influenced days (with ±1 SEM uncertainy) for (a) 1983–2014 accumulated telescope data and (b) 2004–14 AERONET data. The AERONET colors correspond identically to Fig. 10). Weighted least squares regressions are also shown.

5. Conclusions

Daily average atmospheric extinction (τ) has been calculated from several telescope datasets using instruments located on the North Atlantic Canary Archipelago that have recorded data over a period of

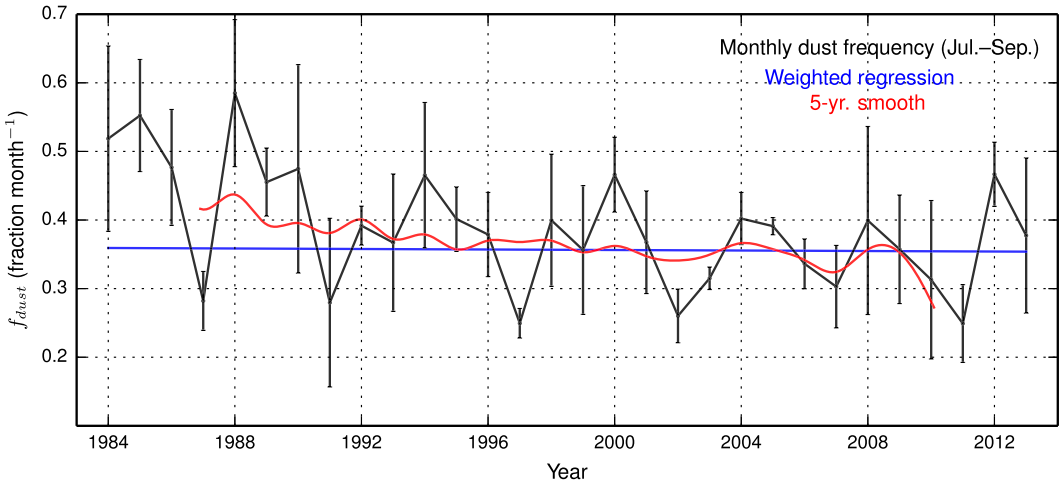

FIG. 15. The f_{dust} (and SEM range) over the July–September period (fraction month^{-1}), calculated from the accumulated telescope data. During this period the exported dust is most frequent at relatively high altitudes (>2400 m), and thus it is most reliably observed by the telescopes relative to other times of the year (as shown in Fig. 9). A 5-yr running mean is overplotted (red line) to highlight long-term changes.

approximately 30 yr. These datasets provide a rare insight into the atmospheric conditions of a site that intersects one of the main pathways of dust export from the Sahara. We have contrasted these data with comparable measurements from NASA's AERONET monitors, although these data cover a much shorter period than those of the telescopes (<10 yr).

By analyzing these data together, we have identified strong evidence of seasonal changes in the height of dust outbreaks—a finding that has enabled us to analyze the long-term changes of the telescope-retrieved τ more effectively. Our subsequent long-term analysis suggested that the frequency of high-altitude (≥2.4 km) dust outbreaks varies from year to year by around 9%, yet there has been no significant change in the events overall.

Acknowledgments. The authors kindly thank Drs. Beatriz González-Merino and Tariq Shahbaz for their comments and discussion. Daffyd Wyn Evans provided the extinction data generated from observations carried out with the Carlsberg Meridian Telescope run by Real Instituto y Observatorio de la Armada en San Fernando, Copenhagen University Observatory, and the Royal Greenwich Observatory. The Mark-1 instrument belongs to the High-Resolution Optical Spectroscopy (HIROS) group of the School of Astronomy and Physics at the University of Birmingham and is a node of the Birmingham Solar Oscillations Network (BiSON). Javier Expossito-Gonzalez, Bahaiddin Damari, and Emilio Cuevas-Agullo established and maintain the Tenerife AERONET sites used in this work (http://aeronet.gsfc.nasa.gov). We gratefully acknowledge the open source tools we have used, the Python language and the IPython project, from the Anaconda Continuum distribution.

REFERENCES

Alonso-Pérez, S., E. Cuevas, and X. Querol, 2011: Objective identification of synoptic meteorological patterns favouring African dust intrusions into the marine boundary layer of the subtropical eastern north Atlantic region. *Meteor. Atmos. Phys.*, **113**, 109–124, doi:10.1007/s00703-011-0150-z.

Brookes, J., G. Isaak, and H. van der Raay, 1978: A resonant-scattering solar spectrometer. *Mon. Not. Roy. Astron. Soc.*, **185**, 1–18, doi:10.1093/mnras/185.1.1.

Cachorro, V., P. Romero, C. Toledano, E. Cuevas, and A. de Frutos, 2004: The fictitious diurnal cycle of aerosol optical depth: A new approach for "in situ" calibration and correction of AOD data series. *Geophys. Res. Lett.*, **31**, L12106, doi:10.1029/2004GL019651.

——, C. Toledano, A. Berjón, A. de Frutos, B. Torres, M. Sorribas, and N. S. Laulainen, 2008: An "in situ" calibration correction procedure (KCICLO) based on AOD diurnal cycle: Application to AERONET–El Arenosillo (Spain) AOD data series. *J. Geophys. Res.*, **113**, D12205, doi:10.1029/2007JD009673.

Cana, L., 2002: The Saharan dust episode of 26 February 2000 over the Canary archipelago: A synoptic overview. *Weather*, **57**, 385–389, doi:10.1256/wea.275.01.

Cortés, T. R., and P. L. Pallé, 2014: The Mark-I helioseismic experiment. I. Measurements of the solar gravitational redshift (1976-2013). *Mon. Not. Roy. Astron. Soc.*, **443**, 1837–1848, doi:10.1093/mnras/stu1238.

Cuesta, J., J. H. Marsham, D. J. Parker, and C. Flamant, 2009: Dynamical mechanisms controlling the vertical redistribution of dust and the thermodynamic structure of the West Saharan atmospheric boundary layer during summer. *Atmos. Sci. Lett.*, **10**, 34–42, doi:10.1002/asl.207.

Evan, A. T., and S. Mukhopadhyay, 2010: African dust over the northern tropical Atlantic: 1955–2008. *J. Appl. Meteor. Climatol.*, **49**, 2213–2229, doi:10.1175/2010JAMC2485.1.

——, C. Flamant, S. Fiedler, and O. Doherty, 2014: An analysis of aeolian dust in climate models. *Geophys. Res. Lett.*, **41**, 5996–6001, doi:10.1002/2014GL060545.

Finkbeiner, D. P., 2003: A full-sky Hα template for microwave foreground prediction. *Astrophys. J. Suppl. Ser.*, **146**, 407–415, doi:10.1086/374411.

García-Gil, A., C. Muñoz-Tuñón, and A. M. Varela, 2010: Atmosphere extinction at the ORM on La Palma: A 20 yr statistical database gathered at the Carlsberg Meridian Telescope. *Publ. Astron. Soc. Pac.*, **122**, 1109–1121, doi:10.1086/656329.

Goudie, A., and N. Middleton, 2001: Saharan dust storms: Nature and consequences. *Earth Sci. Rev.*, **56**, 179–204, doi:10.1016/S0012-8252(01)00067-8.

Guerrero, M., and Coauthors, 1998: Extinction over the Canarian observatories: The limited influence of Saharan dust. *New Astron. Rev.*, **42**, 529–532, doi:10.1016/S1387-6473(98)00066-9.

Hardie, R., 1962: Photoelectric reductions. *Astronomical Techniques*, W. A. Hiltner, Ed., Stars and Stellar Systems, Vol. 2, University of Chicago Press, 178–208.

Janowiak, J. E., 1988: An investigation of interannual rainfall variability in Africa. *J. Climate*, **1**, 240–255, doi:10.1175/1520-0442(1988)001<0240:AIOIRV>2.0.CO;2.

Jiménez, A., H. Gonzalez Jorge, and M. Rabello-Soares, 1998: Diurnal atmospheric extinction over Teide Observatory (Tenerife, Canary Islands). *Astron. Astrophys. Suppl. Ser.*, **129**, 413–423, doi:10.1051/aas:1998193.

King, D., 1985: Atmospheric extinction at the Roque de los Muchachos Observatory, La Palma. Royal Greenwich Observatory La Palma Tech. Note 31, 5 pp.

Knippertz, P., and M. C. Todd, 2012: Mineral dust aerosols over the Sahara: Meteorological controls on emission and transport and implications for modeling. *Rev. Geophys.*, **50**, RG1007, doi:10.1029/2011RG000362.

Krügel, E., 2009: The influence of scattering on the extinction of stars. *Astron. Astrophys.*, **493**, 385–397, doi:10.1051/0004-6361:200809976.

Laken, B. A., H. Parviainen, E. Pallé, and T. Shahbaz, 2014: Saharan mineral dust outbreaks observed over the North Atlantic island of La Palma in summertime between 1984 and 2012. *Quart. J. Roy. Meteor. Soc.*, **140**, 1058–1068, doi:10.1002/qj.2170.

Moulin, C., C. E. Lambert, F. Dulac, and U. Dayan, 1997: Control of atmospheric export of dust from North Africa by the North Atlantic Oscillation. *Nature*, **387**, 691–694, doi:10.1038/42679.

——, and Coauthors, 1998: Satellite climatology of African dust transport in the Mediterranean atmosphere. *J. Geophys. Res.*, **103**, 13 137–13 144, doi:10.1029/98JD00171.

Müller, D., I. Mattis, U. Wandinger, A. Ansmann, D. Althausen, O. Dubovik, S. Eckhardt, and A. Stohl, 2003: Saharan dust over a central European EARLINET-AERONET site: Combined observations with Raman lidar and Sun photometer. *J. Geophys. Res.*, **108**, 4345, doi:10.1029/2002JD002918.

Pallé, P., J. Pérez, C. Régulol, T.-R. Cortésl, G. Isaak, C. McLeod, and H. Van der Raay, 1986: The global oscillation spectrum of the sun. I—Analysis of daily power spectra of velocity measurements. *Astron. Astrophys.*, **169**, 313–318.

Siher, E. A., S. Ortolani, M. S. Sarazin, and Z. Benkhaldoun, 2004: Correlation between TOMS aerosol index and astronomical extinction. *Ground-Based Telescopes*, J. M. Oschmann Jr., Ed., International Society for Optical Engineering (SPIE Proceedings, Vol. 5489), 138–145, doi:10.1117/12.549804.

Swap, R., S. Ulanski, M. Cobbett, and M. Garstang, 1996: Temporal and spatial characteristics of Saharan dust outbreaks. *J. Geophys. Res.*, **101**, 4205–4220, doi:10.1029/95JD03236.

Varela, A. M., J. J. Fuensalida, C. Muñoz-Tuñón, J. M. R. Espinosa, B. M. Garcia-Lorenzo, and E. Cuevas, 2004: Comparison of the aerosol index from satellites and the atmospheric extinction coefficient above the Canarian Observatories. *Ground-Based Telescopes*, J. M. Oschmann Jr., Ed., International Society for Optical Engineering (SPIE Proceedings, Vol. 5489), 245–255, doi:10.1117/12.555854.

——, C. Bertolin, C. Muñoz-Tuñón, S. Ortolani, and J. Fuensalida, 2008: Astronomical site selection: On the use of satellite data for aerosol content monitoring. *Mon. Not. Roy. Astron. Soc.*, **391**, 507–520, doi:10.1111/j.1365-2966.2008.13803.x.

Viana, M., X. Querol, A. Alastuey, E. Cuevas, and S. Rodríguez, 2002: Influence of African dust on the levels of atmospheric particulates in the Canary Islands air quality network. *Atmos. Environ.*, **36**, 5861–5875, doi:10.1016/S1352-2310(02)00463-6.

Westphal, D. L., O. B. Toon, and T. N. Carlson, 1987: A two-dimensional numerical investigation of the dynamics and microphysics of Saharan dust storms. *J. Geophys. Res.*, **92**, 3027–3049, doi:10.1029/JD092iD03p03027.